Broadband chirality and asymmetric transmission in ultrathin 90°-twisted Babinet-inverted metasurfaces

J. H. Shi,[1,2,*] H. F. Ma,[1] C. Y. Guan,[2] Z. P. Wang,[2] and T. J. Cui[1,*]

[1]*State Key Laboratory of Millimeter Waves, Southeast University, Nanjing 210096, China*

[2]*Key Laboratory of In-Fiber Integrated Optics of Ministry of Education, College of Science, Harbin Engineering University, Harbin 150001, China*

(Received 12 November 2013; revised manuscript received 9 April 2014; published 22 April 2014)

A broadband asymmetric transmission of linearly polarized waves with totally suppressed copolarization transmission is experimentally demonstrated in ultrathin 90°-twisted Babinet-inverted metasurfaces constructed by an array of asymmetrically split ring apertures. The only accessible direction-dependent cross-polarization transmission is allowed in this anisotropic chiral metamaterial. Through full-wave simulation and experiment results, the bilayered Babinet-inverted metasurface reveals broadband artificial chirality and asymmetric transmission, with a transmission contrast that is better than 17.7 dB within a 50% relative bandwidth for two opposite directions. In particular, we can modify polarization conversion efficiency and the bandwidth of asymmetric transmission via parametric study.

DOI: 10.1103/PhysRevB.89.165128 PACS number(s): 41.20.Jb, 42.79.Ci, 42.81.Gs

In recent years, metamaterial has attracted growing attention in the scientific communities because it enables researchers to easily design and achieve unprecedented electromagnetic responses of artificial structures [1,2]. For electromagnetic waves, polarization is undoubtedly one of the most important fundamental characteristics. The newly invented anisotropic and chiral metamaterials hold great advantages and flexibilities to manipulate the propagation of electromagnetic waves and particularly to tailor polarization states [3,4]. Since optically active media were promising candidates for negative refraction [5,6], many chiral metamaterials have subsequently been proposed to realize a negative refractive index [7–9]. As the concept goes beyond the negative index, great efforts have been devoted to achieving giant circular dichroism and optical activity in chiral metamaterials [3]. Numerous chiral metamaterial-based polarization devices have been reported, such as polarization rotators, [10] circular polarizers [11–14], and polarization spectrum filters [15,16]. Another intriguing effect in two-dimensional (2D) chiral metamaterial is direction-dependent circular conversion dichroism, leading to an asymmetric transmission phenomenon [17]. The 2D chirality is intrinsically anisotropic. Both planar intrinsically and extrinsically chiral metamaterial patterns can show such a directionally asymmetric total transmission from microwave to optical frequencies [18–22]. In contrast to the nonreciprocal transmission achieved in magneto-optical, nonlinear, or time-dependent media [23], the asymmetric transmission in planar chiral metamaterial is reciprocal and fully compliant with Lorentz's reciprocity theorem. The reciprocal asymmetric transmission effect arises from reversed right-to-left and left-to-right polarization conversion efficiencies for opposite directions of wave propagation. Meanwhile, there have been attempts to achieve the asymmetric transmission for linearly polarized waves [24–31]. A three-dimensional low-symmetry metamaterial without any rotational symmetry showed 25% asymmetric transmission for linearly polarized light [24]. The criterion on the transmission matrix elements for producing the asymmetric transmission only for linearly polarized waves and a microscopic electric Lorentz theoretical description has been presented theoretically [25–27]. It was theoretically found that asymmetric transmission for linear polarizations could be easily achieved by a monolayer of anisotropic chiral metamolecules through the constructive and destructive interferences between the contributions from anisotropy and those from chirality [28]. Further, several metamaterials composed of twisted metamolecules have been reported as having strong asymmetric transmission [26], polarization transformation [29], asymmetric transmission of linearly polarized waves based on combining chirality and electromagnetic wave tunneling [30], and dual-band asymmetric transmission [31] individually for two orthogonal linearly polarized waves. However, some chiral metamaterials are multilayered [29,30], or the asymmetric transmission in other metamaterials strongly depends on wave frequency and only operates in a narrow frequency range [26,30,31]. In addition, undesirable high copolarization transmission deliberately limits polarization conversion efficiency and the bandwidth of asymmetric transmission [3]. The broadband operation of the asymmetric transmission phenomenon with nearly zero copolarization transmission in a simple structured metamaterial is still highly desirable.

In this paper, we propose ultrathin 90°-twisted Babinet-inverted metasurfaces constructed by an array of asymmetrically split ring apertures (ASRAs). The orthogonal arrangement of two stacked Babinet-inverted resonators makes the metamaterial chiral due to cross-coupling between the magnetic and the electric responses. The planar anisotropic chiral metasurface enables a broadband asymmetric transmission of linearly polarized waves, with total suppression of copolarized transmission at the normal incidence. One linearly polarized wave is only allowed to pass through the planar chiral metasurface from one direction and is blocked from the opposite direction.

Asymmetrically split ring (ASR) metamolecules are important building blocks of metamaterial structures for achieving trapped-mode resonances, optical activity, and asymmetric

*Corresponding authors: hrbeusjh@gmail.com and tjcui@seu.edu.cn

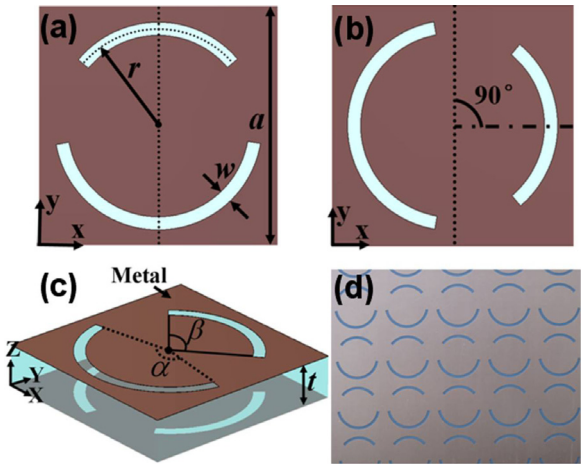

FIG. 1. (Color online) 90°-twisted Babinet-inverted metasurface. The views of the (a) front and (b) back layers. Two ASRAs rotate with respect to each other by a twist angle of 90°. (c) The schematic of a unit cell of the stereo ASRA dimer array. Each ASRA resonator has different arc slits corresponding to angles α and β. Two ASRAs are coaxial. The forward propagation is along the $-z$ direction. (d) The top view of a fabricated Babinet-inverted metasurface sample, which was manufactured from F4B laminates using the photolithography technique.

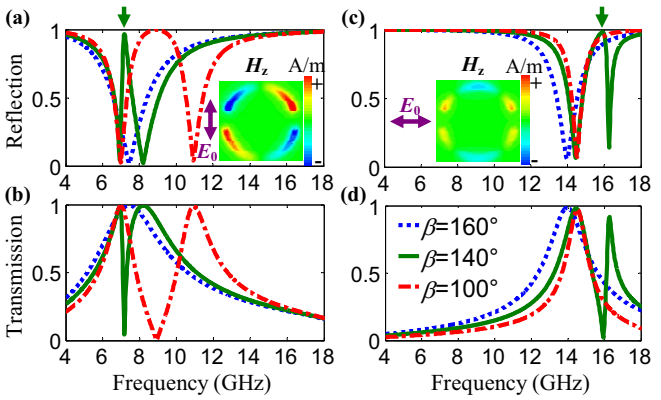

FIG. 2. (Color online) The (a) and (c) reflection and (b) and (d) transmission spectra of the single-layer Babinet-inverted metasurface. The dotted, solid, and dash-dotted lines indicate geometric structures with $\beta = 160°$, $\beta = 140°$, and $\beta = 100°$, respectively, and the other open angle is $\alpha = 160°$. The insets show polarizations of incident waves and z-component magnetic near-field distributions at frequencies marked by bold arrows.

transmission [15,16,20]. Here, the Babinet principle is applied to design the planar chiral metasurface [32–34]. The Babinet-inverted metasurface consists of an array of ASRAs that are exactly complementary to ASRs [16]. The bilayered metasurfaces are geometrically identical but are arranged with a twist angle of 90° in order to give birth to the strongest chirality due to the near-field magnetic and electric coupling, while the bilayered metasurfaces with twist angles of 0° and 180° will not exhibit any chiral property. We can also call the structure a stereometasurface with stereo ASRA dimers. One can expect that the 90°-twisted Babinet-inverted metasurface design efficiently suppresses the copolarization transmission, and equivalently, the signal-to-noise ratio is greatly improved [34], where the signal-to-noise ratio for the transmitted wave is proportional to the ratio of the cross-polarization transmission over the copolarization transmission.

The 90°-twisted Babinet-inverted metasurface configuration is sketched in Fig. 1. This metasurface consists of an array of square stereo ASRA dimers. Each stereo ASRA dimer consists of two spatially separated coaxial ASRAs that are structurally identical, but the back layer is twisted by 90° with respect to the front one. Each ASRA consists of two different arc slits corresponding to open angles α and β (e.g., $\alpha = 160°$ and $\beta = 100°$), as shown in Fig. 1(c). For simplicity, open angle α is constant while β is variable. The radius of the ASRA is $r = 6$ mm, and the split width is $w = 0.8$ mm. Both metasurface patterns, with an overall size of 300×300 mm^2, were perforated from 35-μm copper cladding on the F4B substrate with a thickness of $t = 1.5$ mm. The period of perforation is $d = 15$ mm, rendering the structure nondiffractive at normal incidence for frequencies below 20 GHz. The photograph of a fabricated sample is given in Fig. 1(d).

First, we studied the electromagnetic response of the single-layer Babinet-inverted metasurface. The single-layered ASR metasurface without twofold rotational symmetry can support a so-called trapped-mode resonance mimicking the electromagnetically induced transparency (EIT) phenomenon, in which the polarized wave along the rings could excite a strong magnetic dipole perpendicular to the metasurface plane. Inverting the ASR structure leads to the ASRA one in a continuous metallic film. According to Babinet's principle, instead of an EIT-like enhanced transmission in the ASR metasurface, an enhanced reflection as a counterpart of the EIT [35,36] within the broad spectral profile occurs in the Babinet-inverted metasurface illuminated by light polarized perpendicular to the ring apertures, in which the open angles are $\alpha = 160°$ and $\beta = 140°$, as shown in Fig. 2(a). Here, the transmission spectra and the associated excitation modes were performed using the commercial software CST Microwave Studio, where copper is treated as a perfectly electric conductor and the lossy dielectric substrate is assumed to have a relative permittivity of $\varepsilon = 2.65 + i \cdot 0.003$. The z-component magnetic near-field distribution at the reflection peak shows the characteristic of two out-of-phase oscillating magnetic dipoles in the metasurface plane, thus being a magnetic dark mode. The corresponding trapped mode is weakly coupled to free space. The reflection peak also happens to be illuminated by light polarized parallel to the ring apertures due to excitation of the other low-loss, magnetic, high-order mode, as shown in Fig. 2(c). These dark resonances are normally inaccessible in symmetrically split ring apertures $\alpha = \beta = 160°$, in which only a broad dipole mode can be excited (see dotted lines in Figs. 2(a) and 2(c)). The increasing asymmetry of $\alpha = 160°$ and $\beta = 100°$ leads to a much broader reflection band and a lower absorption. The transmission spectra of the single-layer Babinet-inverted metasurface are presented in Figs. 2(b) and 2(d). It is only transparent within narrow spectral ranges, and the transmission dramatically drops away from the resonant frequencies in a perforated metallic film. In particular, no cross-polarization transmission is observed at normal incidence in such a single-layer metasurface. However, once two ASRA elements are rotated by 90° with respect

to each other, the chirality is created, since two orthogonal eigenmodes will strongly couple with each other through apertures. Such a 90°-twisted Babinet-inverted metasurface modifies four elements of the Jones matrix in an extremely broad band. The only one of two off-diagonal elements is enhanced; three others are suppressed nearly to zero. Consequently, a broadband asymmetric transmission can be achieved.

The copolarization transmission coefficients T_{xx} and T_{yy} coincide well with each other in the 90°-twisted Babinet-inverted metasurface. The complex amplitudes of the incident to the transmitted wave are related by the Jones matrix for the forward-propagating wave along the $-z$ direction:

$$\begin{pmatrix} T_x \\ T_y \end{pmatrix} = \begin{pmatrix} T_{xx} & T_{xy} \\ T_{yx} & T_{yy} \end{pmatrix} \begin{pmatrix} I_x \\ I_y \end{pmatrix} = \begin{pmatrix} \tau & \xi \\ \zeta & \tau \end{pmatrix} \begin{pmatrix} I_x \\ I_y \end{pmatrix} = \mathbf{T}^f_{\text{lin}} \begin{pmatrix} I_x \\ I_y \end{pmatrix} \tag{1}$$

where the superscript refers to the forward (f, along the $-z$ axis) or backward (b, along the $+z$ axis) wave propagations. For the backward-propagating wave along the $+z$ direction, according to the reciprocity theorem, the corresponding matrix is given as follows [24]:

$$\mathbf{T}^b_{\text{lin}} = \begin{pmatrix} \tau & -\zeta \\ -\xi & \tau \end{pmatrix} \tag{2}$$

The asymmetric transmission parameters for linearly polarized waves are then defined as the total intensity difference between two opposite directions (i.e., the intensity difference between two cross-polarization components for the same propagation direction):

$$\begin{aligned} \Delta^x &= |T^f_{xx}|^2 + |T^f_{yx}|^2 - |T^b_{xx}|^2 - |T^b_{yx}|^2 \\ &= |T^f_{yx}|^2 - |T^f_{xy}|^2 = \zeta^2 - \xi^2 \\ \Delta^y &= |T^f_{yy}|^2 + |T^f_{xy}|^2 - |T^b_{yy}|^2 - |T^b_{xy}|^2 \\ &= |T^f_{xy}|^2 - |T^f_{yx}|^2 = \xi^2 - \zeta^2 = -\Delta^x \end{aligned} \tag{3}$$

Due to specific symmetry, although the copolarization transmission τ is not directly included in Eq. (3), high transmission amplitudes of t_{xx} and t_{yy} ($t_{ij} = |T_{ij}|$) will extremely hamper the realization of broadband asymmetric transmission and lead to a large ellipticity of the transmitted wave [30]. According to Eq. (3), we can realize perfect asymmetric transmission ($\Delta^y = -\Delta^x = 1$) under certain conditions. These conditions are (1) complete cross-polarization conversion and (2) unit transmission. The underlying mechanism of the ideal asymmetric transmission stems from the only accessible direction-dependent cross-polarization transmission due to the peculiar polarization eigenstates. For broadband application, these requirements are not easily achievable in a bilayered chiral structure. Most of the area of the Babinet-inverted metasurface is opaque; thus, it can prevent the copolarization transmission [34]. In our case, the 90°-twisted Babinet-inverted metasurface promises that all conditions—$\tau \approx 0$, $\zeta \approx 0$, $\xi \gg \tau$, and $\xi \gg \zeta$—are simultaneously satisfied in a broad frequency range. At some frequencies, the metasurface has a high transmission (i.e., $\xi \approx 1$). The particular feature of the bilayered Babinet-inverted metasurface is verified by the simulated results in Fig. 3(a), where $\alpha = 160°$ and $\beta = 100°$ are preferred due to smaller absorption. For the forward propagation along the $-z$ direction, the copolarization transmissions t_{xx} and t_{yy} are always identical and exhibit three resonant peaks below 0.1. In contrast to the copolarization transmissions, the cross-polarization transmission t_{xy} is extremely different from that of t_{yx} at all frequencies, indicating the presence of the asymmetric transmission effect for linearly polarized waves and the absence of the asymmetric transmission effect for circularly polarized waves in the proposed chiral metamaterial. Clearly, the cross-polarization transmission t_{xy} shows three transmission peaks at ~5.5, 8.25, and 9.9 GHz, reaching maxima of 0.85, 0.96, and 0.93, respectively, while the other cross-polarization transmission, t_{yx}, is below 0.025. In the frequency range from 5.5 to 10 GHz, the transmission contrast between ${t_{xy}}^2$ and ${t_{yx}}^2$ is larger than 27 dB; furthermore, the transmission contrast between ${t_{xy}}^2$ and ${t_{xx}}^2$ (${t_{yy}}^2$) is larger than 18.6 dB. In this broad passband, for the forward propagation, the incident y-polarized wave can pass through the metamaterial slab and then convert to the x-polarized wave while the incident x-polarized wave is blocked.

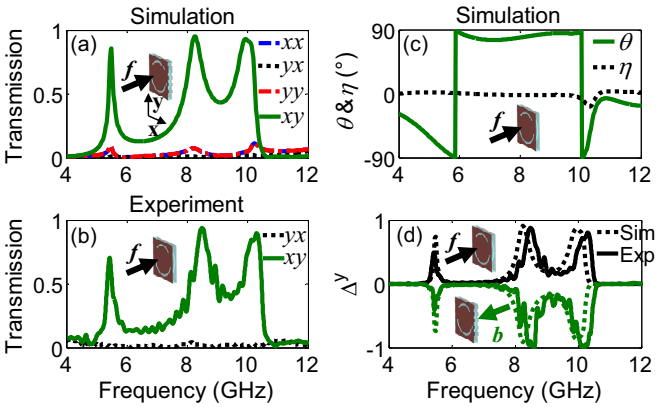

FIG. 3. (Color online) Simulated and measured results of the 90°-twisted Babinet-inverted metasurface with $\alpha = 160°$ and $\beta = 100°$. (a) The simulated transmission spectra t_{xx}, t_{yx}, t_{yy}, and t_{xy} and (b) the simulated polarization rotation angle θ and ellipticity η for a y-polarized forward-propagating wave. The insets indicate wave propagation directions. (c) The measured cross-polarization transmission spectra t_{xy} and t_{yx} for y- and x-polarized forward-propagating waves. (d) The simulated and measured asymmetric transmission parameter Δ^y for forward- and backward-propagating waves, where solid and dotted curves correspond to the measured and the simulated results, respectively.

In terms of the circular transmission coefficient, the polarization state of the transmitted wave can be further studied. The circular transmission matrix can be calculated from the linear transmission matrix

$$\begin{pmatrix} T_{++} & T_{+-} \\ T_{-+} & T_{--} \end{pmatrix} = \frac{1}{2} \begin{pmatrix} T_{xx} + T_{yy} + i(T_{xy} - T_{yx}) & T_{xx} - T_{yy} - i(T_{xy} + T_{yx}) \\ T_{xx} - T_{yy} + i(T_{xy} + T_{yx}) & T_{xx} + T_{yy} - i(T_{xy} - T_{yx}) \end{pmatrix} \tag{4}$$

where + and − denote right-handed and left-handed circularly polarized waves, respectively. The polarization rotation angle θ and its ellipticity angle η are given as follows:

$$\theta = -\frac{1}{2}[\arg(T_{++}) - \arg(T_{--})],$$
$$\eta = \frac{1}{2}\arcsin\left(\frac{|T_{++}|^2 - |T_{--}|^2}{|T_{++}|^2 + |T_{--}|^2}\right) \quad (5)$$

In Fig. 3(b), the transmitted wave is nearly linearly polarized in a broad band since the polarization rotation angle is larger than 77°, accompanied by very low ellipticity ($\eta < 2°$). We also check the polarization state of the transmitted wave based on the polarization conversion ratio (PCR), defined as $PCR = |T_{xy}|^2/(|T_{xy}|^2 + |T_{yy}|^2)$, for the incident y-polarized wave. The PCR is always larger than 0.98 from 5.5 to 10 GHz (not shown in Fig. 2), indicating that the forward y-polarized wave is converted into x-polarized one completely after the transmission.

To verify our prediction and simulations, the cross-polarization transmission and asymmetric parameter were measured at normal incidence in the frequency range from 4 to 12 GHz, as shown in Figs. 3(c) and 3(d). The experiments are carried out in an anechoic chamber using broadband horn antennas and a vector network analyzer. The measured cross-polarization transmission t_{xy} shows three transmission peaks at ~5.43, 8.49, and 10.3 GHz, reaching maxima of 0.70, 0.94, and 0.90, respectively, while the other one, t_{yx}, is much lower than t_{xy}. In the broad frequency range of 5.5–10 GHz, the measured transmission contrast between ${t_{xy}}^2$ and ${t_{yx}}^2$ is always larger than 17.7 dB. We can obtain larger than 50% relative bandwidth for a good asymmetric transmission. The measured results in Fig. 3(c) agree well with simulated ones shown in Fig. 3(a). Figure 3(d) shows an obvious directionally asymmetric transmission between the forward and the backward propagations. Here, $\Delta^y = |T_{xy}^f|^2 - |T_{yx}^f|^2$ for the forward propagation, and the intensity transmission difference $|T_{xy}^b|^2 - |T_{yx}^b|^2$ for the backward propagation is equivalent to Δ^x. Both simulated and measured results demonstrate that the two curves of Δ^y and Δ^x are almost contrary to each other. The 90°-twisted Babinet-inverted metasurface allows y-polarized forward wave transmission and x-polarized backward wave transmission and blocks x-polarized forward wave transmission and y-polarized backward wave transmission. The simulation results present ±0.74, ±0.91, and ±0.87 asymmetry parameters at 5.5, 8.25, and 9.9 GHz, respectively. Experimental results show 0.50, 0.88, and 0.81 asymmetry parameters at 5.43, 8.49, and 10.30 GHz, respectively, for the forward propagation and 0.41, 0.96, and 0.98 asymmetry parameters at 5.44, 8.53, and 10.20 GHz, respectively. The low transmission and asymmetric parameter ~7 GHz are mainly caused by high reflection of the Babinet-inverted metasurface. The difference in amplitude and resonant frequencies may be partly caused by fabrication errors and random noises in experiments and largely influenced by the mismatch between the assumed real and imaginary parts of permittivity and the realistic material parameters. Due to the fact that the intensity transmission of one cross-polarization component is much larger than the other one and two copolarization components and the associated transmitted wave are nearly linearly polarized, it can be concluded that the proposed 90°-twisted Babinet-inverted metasurface has a remarkable advantage for broadband asymmetric transmission for linearly polarized light and can be regarded as a good broadband polarization spectrum filter.

As shown in Fig. 2, the response of the single-layered Babinet-inverted metasurface is greatly affected by the degree of ASRA asymmetry, which is proportional to the value $(\alpha - \beta)/(\alpha + \beta)$, and the quality factor of the EIT-like resonance strongly depends on this parameter. Hence, the asymmetry of the ASRA will affect the in-plane coupling strength between two apertures in the same plane; furthermore, it will slightly change the coupling between two ASRAs due to cavity variation formed between two 90°-twisted Babinet-inverted metasurfaces. The variation of geometric structures alters the near-field distributions of electromagnetic modes, thus affecting the far-field radiative properties of the bilayered Babinet-inverted metasurface. Although the asymmetry (or the thickness of the dielectric layer, discussed next) varies, all t_{xx}, t_{yx}, and t_{yy} are still much smaller than t_{xy} in the frequency range from 5.5 to 10 GHz for the forward-propagating wave; therefore, the fundamental feature of the 90°-twisted Babinet-inverted metasurface almost remains unchanged. Next, we mainly study the dependence of the cross-polarization transmission t_{xy} on the asymmetry of the ASRA for the y-polarized forward-propagating wave instead of the asymmetric parameter. The open angle α is kept constant at 160°, and the other open angle, β, is reduced from 160° to 0° every other 10°. Correspondingly, the asymmetry varies from 0 to 1. The interlayer coupling strength almost remains unchanged due to a fixed 1.5-mm distance between two Babinet-inverted layers. The simulated results in Fig. 4(a) show a clear evolution from three to two peaks of the cross-polarization transmission t_{xy} due to the change of the in-plane coupling strength. When the asymmetry is zero as $\alpha = \beta = 160°$, this nonchiral 90°-twisted Babinet-inverted metasurface exhibits no cross-polarization transmission since two orthogonal modes do not couple with each other due to the twofold rotational symmetry of the metamolecule. Once the symmetry is broken, the 90°-twisted Babinet-inverted metasurface becomes chiral and strong coupling between two orthogonal modes occurs, leading to the cross-polarization transmission. Increasing asymmetry leads to a rapid increase of the cross-polarization transmission. Although all three transmission peaks, labeled first, second, and third in Fig. 4(a), blueshift with reducing β (reducing the sizes of the apertures, i.e., increasing the resonant frequency), the spectral splitting between the first two peaks becomes narrower while that between the second and third peaks becomes broader. The peak transmissions at the first two resonances increase and then are maintained ~0.96 when β is less than 40°. The third resonance reveals a different behavior. Besides the large blueshift of the third transmission peak, the amplitude t_{xy} first increases, reaches a maximum of 0.93, and then decreases to zero as the open angle β is changed from 160° to 0°. The nine metasurface samples with a constant spacer thickness of 1.5 mm were fabricated, where $\beta = 0°, 40°, 60°, 80°, 100°, 120°, 130°, 140°$, and 160°. The measured results in Fig. 4(b) agree well with the simulated ones. For instance, when $\beta = 60°$, three peak values are 0.94, 0.96, and 0.61 when they are at ~6.1, 8.24, and

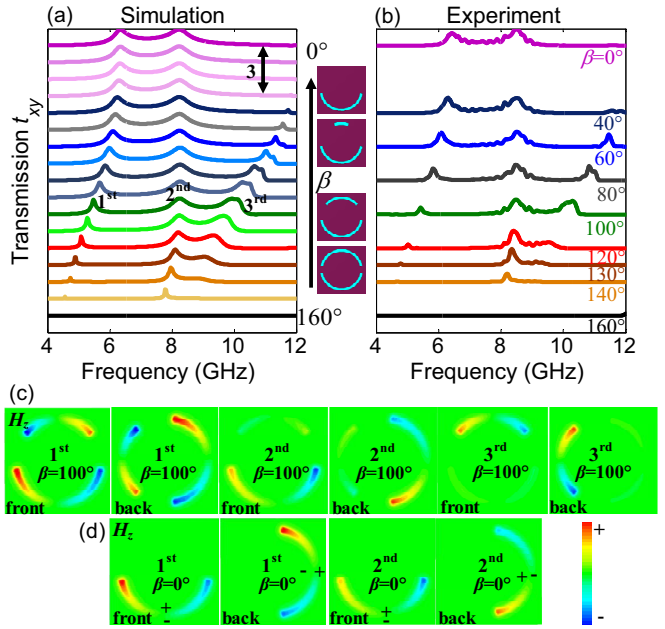

FIG. 4. (Color online) (a) Simulated and (b) measured cross-polarization transmission t_{xy} in the 90°-twisted Babinet-inverted metasurface as a function of the asymmetry of the ASRA. The asymmetry of the ASRA is controlled by the open angle β changing from 160° to 0° in 10° steps, and the other open angle, α, is always 160°, as shown in the inset. The three transmission peaks are denoted as first, second, and third. The nine samples with a constant spacer thickness of 1.5 mm were fabricated, where $\beta = 0°$, 40°, 60°, 80°, 100°, 120°, 130°, 140°, and 160°. (c) and (d) Z-component magnetic near-field distributions and charge distributions of the front and back layers at the first, second, and third transmission peaks for $\beta = 0°$ and 100°. The fields in all maps are plotted in the same scale and recorded 0.2 mm away from the front and back layers. The symbols + and − indicate the surface charge distributions.

11.32 GHz, respectively, in Fig. 4(a) and are 0.87, 0.91, and 0.74 when they are at ∼6.1, 8.52, and 11.50 GHz, respectively, in Fig. 4(b). In order to explore the coupling mechanism and fully recognize the underlying resonant modes in the bilayered Babinet-inverted metasurface, Figs. 4(c) and 4(d) illustrates the z-component magnetic near-field distributions at the three cross-polarization transmission peaks for $\beta = 100°$ and $\beta = 0°$, respectively. Here, it is preferred to study the magnetic rather than the electric near-field distribution in the Babinet-inverted structures [36]. The magnetic fields are recorded 0.2 mm away from the front and back layers. When $\beta = 100°$, three cross-polarization transmission resonances evidently originate from different excitations of ASRAs. The ASRA can be regarded as two-slot dipolar antennas. Excitations of both short and long slot antennas contribute to the first transmission peak, while the second and third transmission peaks are individually dominated by excitations of long and short slot antennas. Clearly, the energy is efficiently transferred from the horizontal apertures in the front layer into the vertical apertures in the back layer at each resonance. In our case, the long slot antenna has a constant length, while the short slot antenna has a variable length. So, it is easily understood that the second transmission peak has less blueshift than the first and third peaks when the open angle β decreases. Maximum magnetic fields near both the front and the back layers at the first and second resonances are recorded at the same time; however, there is nearly a 90° phase delay for recording maximum magnetic fields near the front and back layers at the third resonance. This mentioned phase difference is strongly affected by β. When β is less than 40°, the short aperture barely contributes to the cross-polarization transmission because of no overlap between the short aperture in the back layer and the apertures in the front layer; thus, the third transmission peak vanishes. Therefore, the third transmission peak undergoes exceptional changes. Finally, the cross-polarization transmission spectrum exhibits two peaks when the short apertures disappear. Figure 4(d) records the z-component magnetic near-field distributions of the 90°-twisted Babinet-inverted metasurface with $\beta = 0°$. The excitations of both layers do not suffer from phase delay. The first and second resonances correspond to different excitation modes, respectively. The underlying coupling mechanism can be understood in the resonance hybridization framework [37]. The strong near-field coupling leads to the resonance hybridization in two bilayered metamaterials. The excitation of the vertical apertures in the back layer can be understood as 90°-rotated excitation of the horizontal apertures in the front layer. After the 90° rotation, the z-component magnetic fields are antisymmetric at the first resonance and symmetric at the second resonance, respectively. Varying the asymmetry allows control of the antisymmetric and symmetric modes. Based on the investigations above, it is convenient to engineer the cross-polarization transmission and asymmetric transmission of the 90°-twisted Babinet-inverted metasurface simply by changing the in-plane coupling.

Due to the bilayered structure, the interlayer coupling is another important parameter for modifying the cross-polarization transmission and asymmetric transmission. When the geometric structure remains unchanged as $\alpha = 160°$ and $\beta = 100°$, we can separately consider how the interlayer coupling strength affects the cross-polarization transmission t_{xy}.

The simulated results are shown in Fig. 5(a). The evolution of the transmission peak frequencies due to the thickness

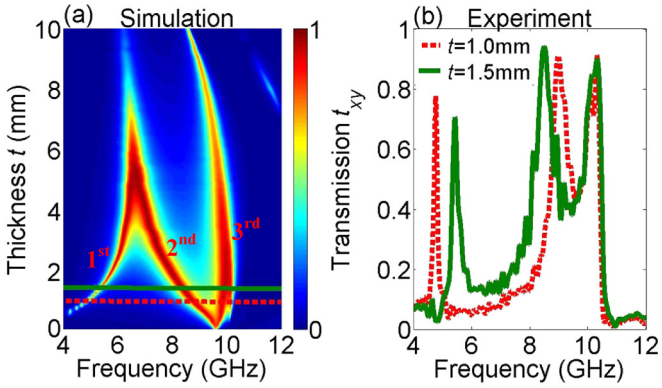

FIG. 5. (Color online) (a) Simulated cross-polarization transmission t_{xy} in the 90°-twisted Babinet-inverted metasurface as a function of dielectric-layer thickness. (b) Measured transmission spectra of two bilayered metamaterials for $t = 1$ and 1.5 mm, denoted by dotted and solid lines, respectively, in Fig. 5(a).

of the spacer layer is similar to the anisotropic three-layer metamaterial discussed in Ref. [38]; however, this unique behavior is applied to the cross-polarization transmission in this paper. When the dielectric-layer thickness is infinitely thin ($t \to 0$), the metasurface reflects all energy in the frequency range of 4–12 GHz and the chirality vanishes. As shown in Fig. 4(c), the first, second, and third resonances can be regarded as an antisymmetric-mode combination for both long and short slot antennas, in which the symmetric mode is for long slot antennas and a phase-modulated symmetric mode is for short slot antennas. The interlayer coupling strength of two orthogonal resonances is proportional to the thickness of the dielectric spacer layer, and the strong coupling in thin metamaterials can make a large spectral splitting between the antisymmetric and the symmetric modes in the mode hybridization scheme [37]. Thus, when the spacer layer is thin, there is a large spectral splitting, where the second and third resonances degenerate at the frequency of the symmetric mode for short slot antennas. With the increasing thickness of the spacer layer, the decreasing coupling strength leads to small spectral splitting; thus, the first and second transmission peaks shift progressively to blue and red with increasing thickness and then merge together when the thickness exceeds 5 mm. The resonances at the back and front layers do not happen simultaneously since the large phase delay occurs in thick metamaterials. The resonant frequency of the third transmission peak is insensitive to the coupling strength and basically locates at ~10 GHz when the thickness is less than 5 mm. The maximum transmission of the first transmission peak rapidly increases with increasing the thickness. Attentively, the maximum transmission of the second transmission peak is nearly 100% and weakly depends on the coupling strength. The third transmission peak seems to have 100% transmission for intermediate coupling strength where an optimal thickness is ~2 mm. Two cross-polarization transmissions become weak and slightly redshift when the thickness is larger than 5 mm. The measured results of the bilayered metasurface with $t =$ 1 and 1.5 mm in Fig. 5(b) are consistent with simulations. As the thickness increases, we observe the blueshift of the first transmission peak, the redshift of the second transmission peak, and no shift of the third transmission peak. In terms of the interlay coupling strength, we can easily manipulate the cross-polarization transmission of the bilayered 90°-twisted Babinet-inverted metasurface.

In conclusion, we have demonstrated theoretically and experimentally that broadband artificial chirality can be realized by an ultrathin 90°-twisted Babinet-inverted metasurface. The orthogonal arrangement of two stacked ASRAs enhances the only the component t_{xy} and nearly suppresses three other ones—t_{xx}, t_{yy}, and t_{yx}—to zero in an extremely broad band. The proposed bilayered metasurface exhibits a broadband asymmetric transmission of a linearly polarized wave with nearly zero copolarization transmission. The bilayered chiral metasurface has been verified to have a transmission contrast that is better than 17.7 dB in the frequency range of 5.5–10 GHz in the experiment. The underlying mechanism of the asymmetric transmission can be well understood as the only accessible direction-dependent cross-polarization transmission. In particular, the 90°-twisted Babinet-inverted metasurface is conveniently engineered based on the in-plane and interlayer coupling strength via changing the geometric asymmetry and the thickness of the spacer layer. We predict that the 90°-twisted Babinet-inverted metasurface with ultralow copolarization noise will be a promising candidate for broadband polarization devices such as spectral filters and beam splitters. Our scheme is also expected to operate in terahertz and infrared ranges.

This paper is supported by the National Science Foundation of China under Grants No. 61201083, No. 61275094, No. U1231201, and No. 613111156; the Natural Science Foundation of Heilongjiang Province in China under Grant No. LC201006; the China Postdoctoral Science Foundation under Grants No. 2012M511171 and No. 2013T60487; the Special Foundation for Harbin Young Scientists under Grant No. 2012RFLXG030; the Fundamental Research Funds for the Central Universities; and 111 Project under Grant No. B13015. H.F.M. and T.J.C. acknowledge support from the National Science Foundation of China under Grants No. 61171024, No. 61171026, No. 60990320, and No. 60990324; National High Tech (863) Projects under Grants No. 2011AA010202 and No. 2012AA030402; and 111 Project under Grant No. 111-2-05.

[1] Y. M. Liu and X. Zhang, Chem. Soc. Rev. **40**, 2494 (2011).
[2] N. I. Zheludev and Y. S. Kivshar, Nat. Mater. **11**, 917 (2012).
[3] Z. F. Li, M. Mutlu, and E. Ozbay, J. Optic. **15**, 023001 (2013).
[4] J. M. Hao, Y. Yuan, L. X. Ran, T. Jiang, J. A. Kong, C. T. Chan, and L. Zhou, Phys. Rev. Lett. **99**, 063908 (2007).
[5] S. Tretyakov, I. Nefedov, A. Sihvola, S. Maslovski, and C. Simovski, J. Electromagn. Waves Appl. **17**, 695 (2003).
[6] J. B. Pendry, Science **306**, 1353 (2004).
[7] E. Plum, J. Zhou, J. Dong, V. A. Fedotov, T. Koschny, C. M. Soukoulis, and N. I. Zheludev, Phys. Rev. B **79**, 035407 (2009).
[8] S. Zhang, Y. S. Park, J. Li, X. Lu, W. Zhang, and X. Zhang, Phys. Rev. Lett. **102**, 023901 (2009).
[9] R. Zhao, L. Zhang, J. Zhou, T. Koschny, and C. M. Soukoulis, Phys. Rev. B **83**, 035105 (2011).
[10] M. Mutlu and E. Ozbay, Appl. Phys. Lett. **100**, 051909 (2012).
[11] J. K. Gansel, M. Thiel, M. S. Rill, M. Decker, K. Bade, V. Saile, G. von Freymann, S. Linden, and M. Wegener, Science **325**, 1513 (2009).
[12] Y. Zhao, M. A. Belkin, and A. Alù, Nat. Comm. **3**, 870 (2012).
[13] S. Yan and G. A. E. Vandenbosch, Appl. Phys. Lett. **102**, 103503 (2013).
[14] H. X. Xu, G. M. Wang, M. Q. Qi, T. Cai, and T. J. Cui, Optic. Express **21**, 24912 (2013).
[15] N. I. Zheludev, E. Plum, and V. A. Fedotov, Appl. Phys. Lett. **99**, 171915 (2011).
[16] J. H. Shi, H. F. Ma, W. X. Jiang, and T. J. Cui, Phys. Rev. B **86**, 035103 (2012).
[17] V. A. Fedotov, P. L. Mladyonov, S. L. Prosvirnin, A. V. Rogacheva, Y. Chen, and N. I. Zheludev, Phys. Rev. Lett. **97**, 167401 (2006).

[18] R. Singh, E. Plum, C. Menzel, C. Rockstuhl, A. K. Azad, R. A. Cheville, F. Lederer, W. Zhang, and N. I. Zheludev, Phys. Rev. B **80**, 153104 (2009).
[19] A. S. Schwanecke, V. A. Fedotov, V. V. Khardikov, S. L. Prosvirnin, Y. Chen, and N. I. Zheludev, Nano Lett. **8**, 2940 (2008).
[20] E. Plum, V. A. Fedotov, and N. I. Zheludev, Appl. Phys. Lett. **94**, 131901 (2009).
[21] L. Wu, Z. Y. Yang, Y. Z. Cheng, M. Zhao, R. Z. Gong, Y. Zheng, J. A. Duan, and X. H. Yuan, Appl. Phys. Lett. **103**, 021903 (2013).
[22] Z. Li, M. Gokkavas, and E. Ozbay, Adv. Opt. Mater. **1**, 472 (2013).
[23] D. Jalas, A. Petrov, M. Eich, W. Freude, S. Fan, Z. Yu, R. Baets, M. Popovic, A. Melloni, J. D. Joannopoulos, M. Vanwolleghem, C. R. Doerr, and H. Renner, Nat. Photon. **7**, 579 (2013).
[24] C. Menzel, C. Helgert, C. Rockstuhl, E. B. Kley, A. Tünnermann, T. Pertsch, and F. Lederer, Phys. Rev. Lett. **104**, 253902 (2010).
[25] M. Kang, J. Chen, H. Cui, Y. Li, and H. Wang, Optic. Express **19**, 8347 (2011).
[26] C. Huang, Y. J. Feng, J. M. Zhao, Z. B. Wang, and T. Jiang, Phys. Rev. B **85**, 195131 (2012).
[27] A. V. Novitsky, V. M. Galynsky, and S. V. Zhukovsky, Phys. Rev. B **86**, 075138 (2012).
[28] S. Zhang, F. Liu, T. Zentgraf, and J. Li, Phys. Rev. A **88**, 023823 (2013).
[29] J. Han, H. Q. Li, Y. C. Fan, Z. Y. Wei, C. Wu, Y. Cao, X. Yu, F. Li, and Z. S. Wang, Appl. Phys. Lett. **98**, 151908 (2011).
[30] M. Mutlu, A. E. Akosman, A. E. Serebryannikov, and E. Ozbay, Phys. Rev. Lett. **108**, 213905 (2012).
[31] J. H. Shi, X. C. Liu, S. W. Yu, T. T. Lv, Z. Zhu, H. F. Ma, and T. J. Cui, Appl. Phys. Lett. **102**, 191905 (2013).
[32] F. Falcone, T. Lopetegi, M. Laso, J. Baena, J. Bonache, M. Beruete, R. Marques, F. Martin, and M. Sorolla, Phys. Rev. Lett. **93**, 197401 (2004).
[33] M. Zalkovskij, R. Malureanu, C. Kremers, D. N. Chigrin, A. Novitsky, S. Zhukovsky, P. T. Tang, P. U. Jepsen, and A. V. Lavrinenko, Laser Photon. Rev. **7**, 810 (2013).
[34] X. Ni, S. Ishii, A. V. Kildishev, and V. M. Shalaev, Light Sci. Appl. **2**, e72 (2013).
[35] N. Liu, T. Weiss, M. Mesch, L. Langguth, U. Eigenthaler, M. Hirscher, C. Sonnichsen, and H. Giessen, Nano Lett. **10**, 1103 (2010).
[36] M. Hentschel, T. Weiss, S. Bagheri, and H. Giessen, Nano Lett. **13**, 4428 (2013).
[37] B. Kanté, S. N. Burokur, A. Sellier, A. de Lustrac, and J. M. Lourtioz, Phys. Rev. B **79**, 075121 (2009).
[38] W. Sun, Q. He, J. M. Hao, and L. Zhou, Optic. Lett. **36**, 927 (2011).